Solvent-Free Mechano-Thermal Synthesis of a Li-Zn Phosphonate Cathode Framework

Augustin Ramackers,[a] Darsi Rambabu,[a],* Tom Goossens,[a] Vasudeva Rao Bakuru,[a] Petru Apostol,[a] Robert Markowski,[a] Géraldine Chanteux,[a] Guillaume Esser,[a] Nicolas Malherbe,[a] Yan Zhang,[a] Fabio Lucaccioni,[a] Yaroslav Filinchuk[a] and Alexandru Vlad [a],*

Dedication: We dedicate this work to God, with gratitude and reverence

[a] Institute of Condensed Matter and Nanosciences, Université catholique de Louvain, 1348 Louvain-la-Neuve, Belgium.

E-mail: *corresponding authors: rambabu.darsi@uclouvain.be & alexandru.vlad@uclouvain.be

Abstract: A key challenge in synthesizing alkali-ion metal–organic frameworks (MOFs) lies in the multi-step procedures typically required, often involving solvothermal crystallization, desolvation, post-synthetic alkali-metalation, and controlled drying. To address this, we report a one-pot, solvent-free mechano-thermal method that combines solid-state grinding of precursors with thermal annealing under vacuum. This direct, scalable route offers a more sustainable alternative while enabling stoichiometric precision. We demonstrate this approach for the synthesis of Li_4-Zn-*p*-DOBDP_mt (LZP^3; *p*-DOBDP^{6-} = 2,5-dioxido-1,4-benzenediphosphate), in which lithium is incorporated during MOF formation. The resulting material exhibits enhanced crystallinity compared to its conventionally synthesized counterpart and retains its key functional properties, including a reversible capacity of 130 mAh/g at 3.2 V vs. Li^+/Li and a quasi-solid-state ionic conductivity of 10^{-6} S/cm at 303 K. These results underscore the viability of solid-state synthesis for constructing alkali-ion-containing organic electrode materials with reduced processing complexity.

Introduction

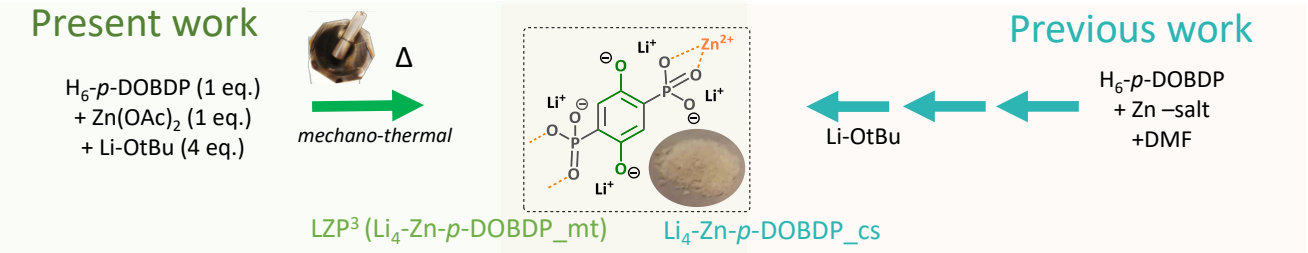
Metal-Organic Frameworks (MOFs) are promising electrode materials for next-generation electrochemical energy storage due to their structural tunability, compositional versatility, and stability. [1–7] Their ability to store charges via both metal centers and organic ligands contributes to high gravimetric energy densities.[8,9] The porous nature facilitates efficient ion transport, while the extended framework provides cycling stability.[7] MOFs can be tailored for electronic, ionic, or mixed conductivity, reducing the need of conductive additives and supporting rapid charge-discharge kinetics. [1,7,10,11] In alkali-ion storage, they have been investigated as both cathodes and anodes. [3–6,10,12,13] While anodes can achieve high capacities, challenges remain in optimizing redox potential, minimizing voltage hysteresis, and improving the coulombic efficiency of the first-cycle.[4,6] Developing MOF-based cathodes is more complex, requiring careful structural and compositional adjustments to enhance electrochemical properties.

Despite progress in MOF-based cathodes, alkali-ion-containing MOFs are still limited. [1,2,7] Their redox activity typically stems from either the anionic framework or metal nodes, while alkali cations primarily act as charge compensators. Only a few such MOFs have been reported, emphasizing the need for further investigation. One of

the earliest examples, Li_2-M-DOBDC (M = Mn, Mg),[1] exhibited a one-electron redox process per ligand at 3.2 V *vs.* Li^+/Li. Structurally, Li_2-Mn-DOBDC is closely related to Mg(Li_2)-p-DHT,[14] whereas Li_2-Mg-DOBDC[1] adopts a different polymorph. The Li_2-Mn-DOBDC MOF demonstrated a conductivity of 10^{-7} S/cm at 293 K, significantly higher than its Mg analogue, highlighting the influence of redox-active metal ions. Later, Li_x-M-(O)-DOBDC (M = Al^{3+}, Fe^{3+}) incorporated trivalent metals, forming Li_3-M-(O)-(DOBDC) or MIL-53(M)-$(OLi)_2$[2] revealed a slightly lower redox potential of 2.76 V *vs.* Li^+/Li. Recently, hexa anionic para-phosphono-phenolate-based (P^3 = *p*-$DOBDP^{6-}$ = 2,5-dioxido-1,4-benzenediphosphate) linker have emerged as a promising alternative, a study on Li_4-Zn-*p*-DOBDP,[7] containing a non-redox-active metal, supports a two-electron redox process per ligand at 3.2 V *vs.* Li^+/Li. It also exhibits Li-ion conductivity (10^{-5} S/cm at 303 K), advancing MOF-based cathode materials. However, limitations persist, including improving electronic conductivity, enhancing alkali-ion transport, and stabilizing high-voltage redox processes.

A key challenge in synthesizing alkali-ion-containing MOFs,[1,2,7] metal-organic compounds (e.g., Li_2-M-p-DHT),[14] and coordination polymers (e.g., Li_2-Co-PTtSA)[15] lies in the multi-step process, which typically involves MOF synthesis, desolvation, alkali-metalation, and drying. These steps often require solvents and careful optimization. In particular, proton exchange in polyanionic frameworks typically requires strong bases (pKa > 14), but solvent-based alkaliation often remains challenging[2,7] due to equilibrium constraints and possible reversibility. To simplify the synthesis, address metalation challenges and eliminate solvent use, a mechano-thermal approach can be employed, wherein the formation of volatile by-products and subsequent thermal treatment under vacuum drive the reaction toward the desired metallated products. Herein, we apply the mechano-thermal approach to synthesize LZP[3] (Li_4-Zn-*p*-DOBDP_mt), achieving direct lithiation during MOF formation, as confirmed by XRD. This one-pot method enhances crystallinity while delivering comparable electrochemical performance (130 mAh/g at 3.2 V *vs.* Li^+/Li) and quasi-solid-state ionic conductivity (10^{-6} S/cm). While this approach is promising for electrode material synthesis, parameters such as annealing temperature and precursor selection must be carefully optimized due to the unidirectional reaction pathway.

This one-step, solvent-free solid-state process offers a sustainable alternative while enabling precise stoichiometric control (**Scheme 1**). Additionally, it circumvents challenges associated with conventional solvothermal methods, such as high solvent consumption, extended reaction times, and limited scalability. However, this approach is restricted to metal salts or bases that generate volatile by-products, necessitating careful precursor selection.[16]



Scheme 1. Comparison of synthesis routes, highlighting the present one-pot solid-state mechano-thermal method (left) versus conventional MOF-based approach (right).

Experimental

Materials (Chemicals and Reagents):

The following chemical were used without further purification: 2,5-Dihydroxy-1,4-benzenediphosphonic acid (H_6-*p*-DOBDP, 98%, Epsilon Chimie), Zinc (II) acetate (99%, anhydrous, Thermo Scientific), Lithium tert-butoxide (Li-OtBu, 97%, Sigma Aldrich), Zinc Nano powder (99%, Sigma Aldrich) Diethylzinc (ca. 15% in Toluene, ca. 1mol/L, TCI). Methanol, THF, DMF solvents (anhydrous, Thermo Scientific), and Polytetrafluoroethylene (PTFE, from Sigma Aldrich).

Physico-Chemical Characterization:

Fourier transform Infra-Red (FTIR) spectroscopy was carried out using an Agilent Technologies Cary 630 FTIR spectrometer operated in transmission or ATR mode. Powder X-ray diffraction (PXRD) patterns were collected either on STOE DARMSTADT Transmission diffractometer system using Mo Kα1 radiation with a wavelength of 0.70930 Å or a MAR345 image-plate detector equipped with an Incoatec Mo (λ = 0.71073 Å) Microfocus (IμS 2.0) X-ray source operating at 50 kV and 1000 μA. The resulting two-dimensional images were azimuthally integrated using the Fit2D software, with LaB6 serving as a calibrant. The XRD samples were loaded into 0.7 mm glass capillaries (Hilgenberg GmbH). SEM images were acquired on Zeiss Neon 40 cross-beam workstation with Gemini SEM column (Carl Zeiss Iberia, S.L, Madrid, Spain). Inductively coupled plasma-optical emission spectrometry (ICP-OES) analysis was performed on Perkin Elmer™ Avio220 max.

Synthesis of LZP^3:

The synthesis was carried out according to the protocol outlined below, with additional optimizations provided in the Supporting Information (SI). All manipulations were performed in an Ar-filled glove box. To a mortar, 1 equivalent of H_6-*p*-DOBDP (0.2 mmol, 54 mg), 1 equivalent of $Zn(OAc)_2$ (0.2 mmol, 37 mg, dried at 180 °C, 5h, prior to use), and 4 equivalents of LiOtBu (0.8 mmol, 64 mg) were added and ground for 15 minutes. The resulting powder was then pressed into a pellet (10 mm) under a pressure of 4 tons for 3 minutes (1 minute per cycle, repeated 3 times). The obtained pellet was subsequently heated in a vacuum oven according to the following temperature program: 5 hours at 160°C, 8 hours at 200°C, and 4 hours at 250°C. After heating, the product, which was off-white, directly yielded the desired LZP^3.

Ionic Conductivity Measurements:

Approximately 20 mg of the powders, with 5 μL of propylene carbonate (PC), were cold-pressed under an applied pressure of 2 tons between two stainless steel rods (7 mm in diameter). These pellets were then placed in custom-designed Swagelok cells, under an inert atmosphere, with the cell locked to maintain the pressure. Variable temperature conductivity measurements were conducted in a climatic chamber with continuous pressure applied. A Bio-Logic potentiostat was used for the conductivity measurements, which included Potentiostatic Electrochemical Impedance Spectroscopy (PEIS) over a frequency range of 7 MHz to 10 mHz with a 200 mV amplitude AC signal. The ionic conductivity was calculated using the equation: $\sigma=L/(AR)$, where σ is the ionic conductivity, L is the thickness of the pellet, A is the pellet area, and R is the resistance obtained from the PEIS data.

Electrochemical Li-metal Half-Cell Assembly and Testing

LZP^3 electrode materials were tested using a two-electrode configuration in 2032-type coin cells, assembled in an Ar-filled glove box. The positive working electrode (cathode) was prepared by hand-grinding 100 mg of Li_4-Zn-*p*-DOBDP_s active material (60 wt.%) with 30 wt.% Super-P carbon (C-65) and 10 wt.% poly(tetrafluoroethylene) (PTFE) dry binder. Approximately 4 mg of the positive electrode composite was then applied onto the stainless-steel positive cell case and pressed directly onto the case using a stainless-steel rod. A glass fiber separator (19 mm diameter) was placed on top of the positive electrode, and 100 μL of electrolyte (1 M $LiPF_6$ in a 1:1 (v/v) mixture of ethylene carbonate and dimethyl carbonate (EC/DMC, LP30, battery-grade, Solvionic)) was added to soak the separator. The Li metal chip, serving as the counter and pseudo-reference electrode (anode), was placed on top of the separator. A stainless steel (316) current collector and spring were placed above the anode, and the cell was sealed with the negative case by applying 0.7 tons of pressure. Galvanostatic charge-discharge tests were conducted at room temperature using a Neware battery testing system.

Results and Discussion

Synthesis, Physico-Chemical Analysis of LZP^3

A solvent-free, single step, mechano-thermal approach was employed to synthesize **LZP^3** (**Scheme 1, left**). Lithium tert-butoxide (Li-OtBu) was chosen as the Li source due to its melting point being within the range of ligand degradation range, making it suitable for solid-state synthesis. Various Zn precursors were tested, including diethylzinc ($Zn(Et)_2$), Zn-metal nano powder and zinc acetate [$Zn(OAc)_2$]. Initially, LZP^3 was synthesized using a 4:1:1 molar ratio of Li:Zn:H_6-*p*-DOBDP, while varying the Zn precursor (**Table S1**). The extent of H–metal exchange (i.e., coordination of Zn and Li) was monitored by FT-IR spectroscopy, with successful metalation indicated by the disappearance of the O–H stretching band at ~3300 cm^{-1}, corresponding to phenolic and phosphonic –OH groups. Diethylzinc, and Zn-nanopowder resulted in partial deprotonation, indicating an incomplete reaction (**Figure 1A**). In contrast, the use of $Zn(OAc)_2$ led to complete disappearance of the O–H stretching band, signifying full deprotonation and effective metalation. The FT-IR spectrum of the sample synthesized using $Zn(OAc)_2$ closely resembles that of the conventionally synthesized MOF prepared in solution (Li_4-Zn-*p*-DOBDP_cs) (**Table S1, Figure 1A)**. The PXRD pattern of LZP^3 is analogous to the reported material Li_4-Zn-*p*-DOBDP_cs, presenting several intensity variations of the main diffraction peaks. For instance, the peak at 5.7° 2theta exhibits significantly higher intensity, while others such as those at 9.7, 10.1°, show improved resolution due to peak separation. Overall, the resulting diffractogram indicates improved crystallinity, likely due to fewer structural defects and possible preferred orientation of the structure (**Figure 1B, 2A**).

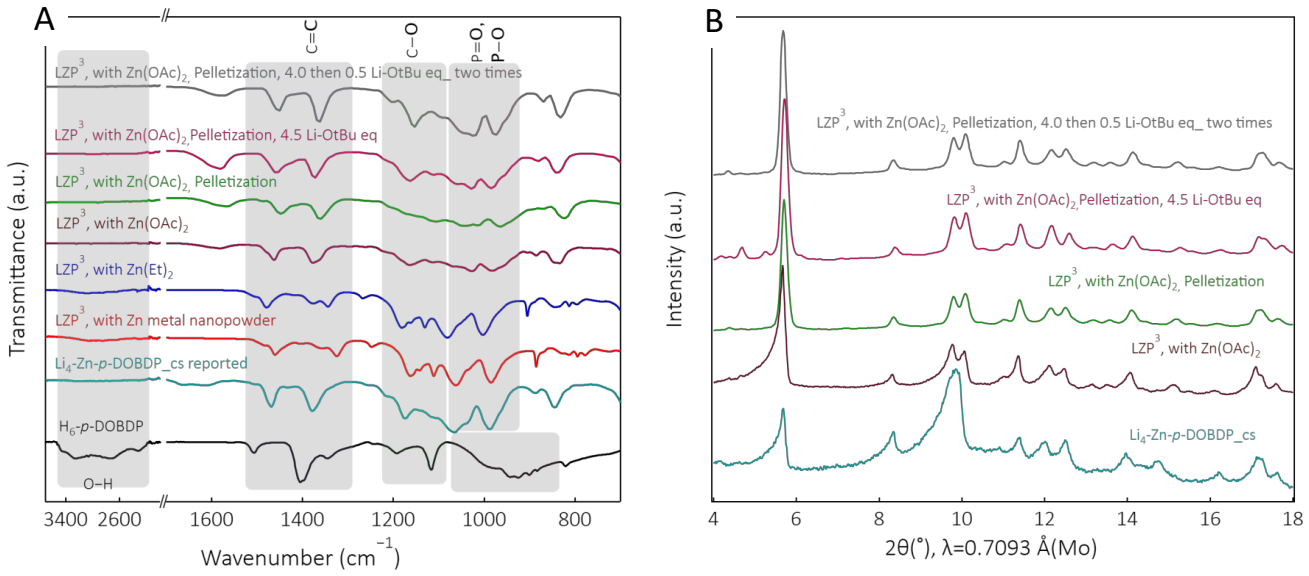


Figure 1. Optimization of the mechano-thermal synthesis of LZP^3. (A) FTIR spectra comparing different Zn precursors and synthetic conditions using $Zn(OAc)_2$ for LZP^3 formation, shown alongside Li_4-Zn-*p*-DOBDP_cs and the H_6-*p*-DOBDP ligand. (B) XRD patterns showing the effect of synthetic parameters using zinc acetate on LZP^3 formation, compared with Li_4-Zn-*p*-DOBDP_cs. All samples were ground for 15 minutes prior to thermal treatment.

The effect of grinding time was evaluated between 10 to 30 minutes, with FT-IR spectra showing comparable features across the range (**Figure S1**). Based on these observations, a grinding time of 15 minutes was considered as optimal. The influence of pelletization was subsequently assessed by comparing samples pelletized under 4 tons of pressure for 3 minutes with those subjected to manual grinding for 15 minutes. XRD analyses indicated that both approaches led to the formation of the same phase. While the XRD peak positions remained consistent, a slight increase in peak intensity was observed for the pelletized sample, suggesting marginally improved crystallinity (**Figure 1B**). Further, Effective metalation was further assessed by inductively coupled plasma optical

emission spectroscopy (ICP-OES), confirming successful solid-state lithiation (**Table S2**). The analysis revealed a Zn-to-Li ion ratio of 1:3.69, which is slightly lower than both the expected ratio (1:4) and the initial precursor ratio. This discrepancy can be attributed to the tendency of lithium tert-butoxide (Li-OtBu) sublimation during the reaction. To compensate this loss, we introduced a slight excess of 4.5 equivalents of Li-OtBu relative to Zn (instead of 4 equivalents required for the stoichiometric ratio). Under these conditions, ICP-OES showed an improved Zn-to-Li ratio of 1:3.93. Furthermore, to improve lithiation efficiency and demonstrate the flexibility of the method, we explored a sequential approach. The reaction was first performed with 4 equivalents of Li-OtBu to yield ($L_{3.69}ZP^3$). Then, an additional 0.5 equivalents of Li-OtBu was added before a second grinding and heating step to compensate for any lithium loss during processing. ICP-OES analysis confirmed enhanced lithiation, with the Zn-to-Li ratio increasing to1:3.98.

The similarity in FT-IR and XRD patterns among $Li_{3.69}ZP^3$ (4 eq. of Li-OtBu used), $Li_{3.93}ZP^3$ (4.5 eq. of Li-OtBu used), and $Li_{3.98}ZP^3$ (4 + 0.5 eq. of Li-OtBu used in two steps) suggests the formation of the same structure, despite a difference of approximately 0.3 equivalents of Li per Zn ion (**Figure 1 and Table S2**). However, in samples where excess Li-OtBu (4.5 equiv.) was used, either in a single step or sequentially, a minor additional peak appeared around 5° 2theta (**Figure 1B**), which may be attributed to unidentified phase impurities. Among these, $L_{3.69}ZP^3$ (with 4.0 equivalents of Li-OtBu, 15 minutes of mechanical grinding, pelletized) was identified as the optimal composition, while others involved either two-step lithiation ($Li_{3.98}ZP^3$) or exhibited minor phase impurities ($Li_{3.93}ZP^3$).

Even though the FT-IR spectrum of the sample synthesized using Zn-acetate closely resembles that of the reported MOF, a notable difference is the presence of a band at 1600 cm^{-1}, which is likely attributed to a C=O stretching vibration introduced during the one-pot synthesis (**Figure 1A)**. This suggests that the band originates from the residual acetate present within framework. In order to remove residual acetate, $L_{3.69}ZP^3$ was washed separately with DMF, THF or methanol. Methanol washing effectively removed the acetate, as confirmed by the disappearance of the C=O band at 1600 cm^{-1} in the FT-IR spectrum (**Figure S2A**). However, methanol washing also carries the risk of partial reprotonation due to its comparable pKa to that of the deprotonated sites in the framework. This reprotonation was confirmed by ICP-OES, showing a loss of lithium ion (Zn:Li ratio of 1:3.25, **Table S2**). The loss of lithium could potentially influence electrochemical performance (*vide infra, Electrochemical Cycling section*). In contrast, THF and DMF washing did not alter the FT-IR spectrum, indicating no significant removal of residual acetate. Powder XRD analysis confirmed that the crystal structure remained unchanged after methanol washings (**Figure S2B**), indicating that residual acetate species may be encapsulated within the framework and are not easily removed by conventional washing.

Furthermore, crystallite size and morphology were examined using scanning electron microscopy (SEM) of Li_4-Zn-*p*-DOBDP_s synthesized under different conditions: without pelletization, with pelletization followed by methanol washing, and with 4.5 equivalents of Li-OtBu. All samples exhibit similar morphologies, consisting of near-spherical particles ranging from approximately 0.5 to 2 µm, forming aggregated structures (**Figure S3**). These results suggest that the morphology remains largely unaffected by pelletization, excess lithiation, or post-synthetic methanol washing. In contrast, the reported (Li_4-Zn-*p*-DOBDP_cs) MOF [7] displays tends toward more plate- or rod-like particles of around 1µm in size. These morphological differences may subtly influence key material properties such as crystallinity (XRD features), electrochemical behavior, and ionic conductivity.

To further confirm the isomorphous nature $Li_{3.93}ZP^3$ to the Li_4-Zn-*p*-DOBDP_cs, the material was treated with 4 equivalents of *p*-toluenesulfonic acid (TsOH) in DMF to induce re-protonation and re-solvation. This treatment yielded a solvated crystalline MOF, H_4-Zn-*p*-DOBDP·DMF_2, whose FT-IR and PXRD patterns matched those of

the conventionally synthesized material (**Figure 2A, 2B**). This confirmed that the framework obtained through solid-state synthesis is isostructural to the previously reported one, with improved crystallinity. A shift in the low-angle peak from 5.7° in LZP[3] to 4.0° in H_4-Zn-*p*-DOBDP·DMF_2 suggests a contraction of the framework in LZP3, consistent with the behavior of Li4-Zn-*p*-DOBDP_cs. Also, profile fitting further confirms reduced unit cell dimensions along the a, b, and c axes in LZP[3] compared to H_4-Zn-*p*-DOBDP·DMF_2. These observations indicate that LZP[3] adopts a more compact framework (**Table S3**, **Figure S4**), a trend that may also be applicable to the isomorph Li_4-Zn-*p*-DOBDP_cs.

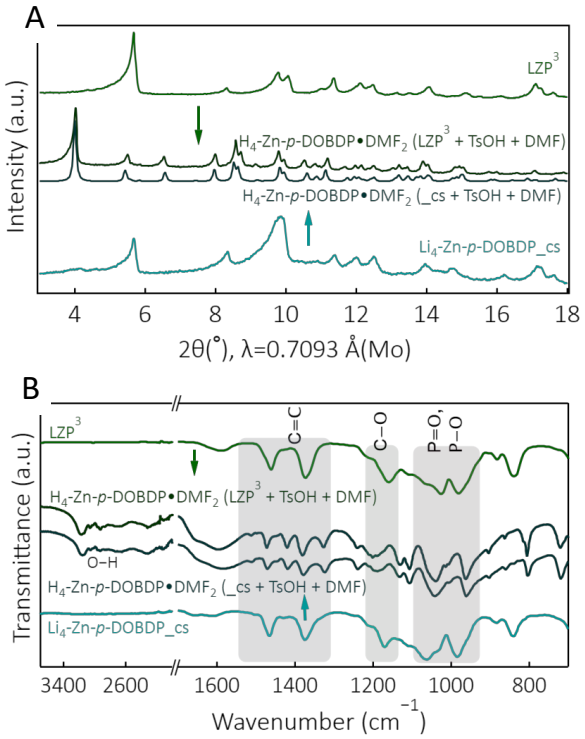


Figure 2. Reprotanation observations of Li_4-Zn-*p*-DOBDP_cs and LZP[3] isomorphs. (A) XRD patterns and (B) FT-IR spectra overlays of Li_4-Zn-*p*-DOBDP_cs, $Li_{3.69}ZP^3$ and their reprotonated MOFs, H_4-Zn-*p*-DOBDP·DMF_2.

Ionic Conductivity of LZP[3]

Motivated by the ionic conductivity reported for lithium-rich Li_4-Zn-*p*-DOBDP_cs, which is crucial for charge–discharge kinetics, we further measured the ionic conductivity of LZP[3] using PEIS (Potentiostatic Electrochemical Impedance Spectroscopy) with a two-probe cold-pressed pellet set-up. No ionic conductivity was observed in the pure solid state, while the reported value for Li_4-Zn-*p*-DOBDP_cs is 10^{-8} S/cm. However, at 303 K and under inert conditions in the quasi-solid state (refer experimental section for details), the ionic conductivity of LZP[3] was found to be 10^{-6} S/cm (**Table 1**), which is one order of magnitude lower than the reported values. Variable-temperature PEIS results (**Figure 3**) for $Li_{3.69}ZP^3$, and $Li_{3.93}ZP^3$, show a comparable activation energy of 0.24 eV, and 0.20 eV, respectively (**Figure 3A, Table 1**). These values are slightly higher than those reported, indicating that the LZP[3] samples exhibit marginally lower conductivity, possibly due to morphological differences (**Figure S3**).

Table 1. Quasi solid Li-ion conductivity, and activation energy of LZP^3 and Li$_4$-Zn-*p*-DOBDP_cs.		
Entry	σ, (S/cm)[a] With PC	E_a, (eV)[b]
$Li_{3.69}ZP^3$ (with 4 eq. Li-OtBu)	1.4 X 10^{-6}	0.24
$Li_{3.93}$ ZP^3 (with 4.5 eq. Li-OtBu)	1.2 X 10^{-6}	0.20
Li$_4$-Zn-*p*-DOBDP_cs (reported)[7]	2.7 X 10^{-5}	0.16
[a] Ionic conductivity at 303 K. [b] Activation energy.		

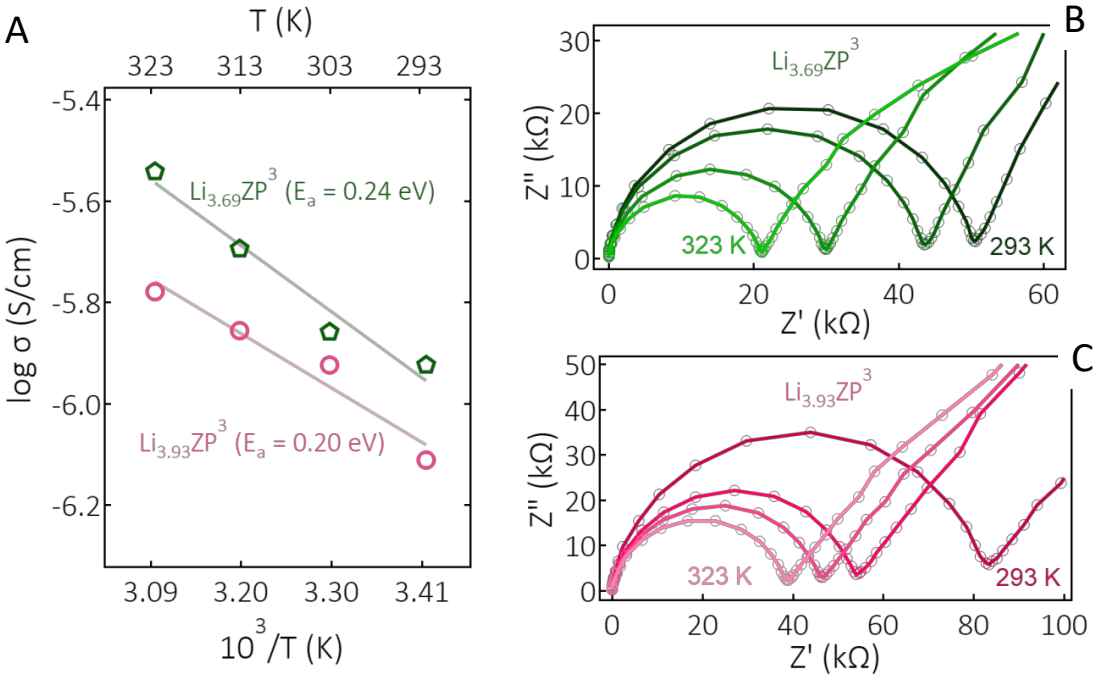


Figure 3. Variable-temperature ionic conductivity plots for LZP^3. (A) Arrhenius plots with corresponding activation energies (E_a). (B, C) Potentiostatic electrochemical impedance spectroscopy (PEIS) results for $Li_{3.69}ZP^3$, and $Li_{3.93}ZP^3$, respectively.

Electrochemical Evaluation of LZP^3

The LZP^3 samples with different contents of lithium, optimized through synthesis adjustments, were evaluated in Li-half cell configurations. The material has a theoretical capacity of 150 mAh/g, corresponding to a 2e$^-$ redox process. The previously reported Li$_4$-Zn-*p*-DOBDP_cs exhibited a specific capacity of 140 mAh/g (1.86e$^-$) at an average potential of 3.2 V vs. Li^+/Li (**Figure 4A**).[7] The first optimized sample, $L_{3.69}ZP^3$, demonstrated an average potential of 3.2 V vs. Li^+/Li, delivering a specific capacity of 130 mAh/g, corresponding to 1.72e$^-$ (**Figure 4B**). In contrast to $L_{3.69}ZP^3$ material, $L_{3.98}ZP^3$ and $L_{3.93}ZP^3$ exhibited specific capacities of 131 mAh/g and 70 mAh/g, corresponding to 1.75e$^-$ and 0.9e$^-$ per formula unit (**Figure S5A, B**). These results indicate that the addition of excess lithium source during synthesis does not enhance electrochemical performance.

Despite the presence of residual acetate in $L_{3.69}ZP^3$, electrochemical cycling remained stable, indicating that post-synthetic washing is unnecessary, and that trace acetate does not significantly affect the electrochemical performance. In fact, methanol washing led to a nearly 50% decrease in capacity, attributed to lithium loss (**Figure**

S5C). Among the samples, $L_{3.69}ZP^3$ exhibited the most favorable electrochemical response. Nevertheless, its capacity remained slightly lower (~9%) than that of the conventionally synthesized Li_4-Zn-*p*-DOBDP_cs. Li-half cells were tested at a 0.025C rate, in contrast to the 0.1 C rate previously reported for Li_4-Zn-*p*-DOBDP_cs. Additionally, 20% less carbon was used in the $L_{3.69}ZP^3$ electrode formulation to align with practical material loading considerations.

To ensure a more complete capacity response, a lower C-rate was employed, as electrochemical behavior can be influenced by factors such as morphology, particle size, and crystallinity.[17] While $L_{3.69}ZP^3$ shows improved crystallinity, it exhibits kinetic limitations likely related to its particle morphology and size distribution, which may hinder ion transport and contribute to a modest reduction in capacity. Ionic conductivity measurements further suggest that limited ionic transport plays a significant role in the observed behavior. Specifically, $L_{3.69}ZP^3$ displays lower ionic conductivity than Li_4-Zn-*p*-DOBDP_cs, which likely contributes to its reduced electrochemical response. This difference is supported by SEM analyses, which reveal that $L_{3.69}ZP^3$ possesses a broader range of particle morphologies and crystallite sizes compared to Li_4-Zn-*p*-DOBDP_cs (**Figure S3**).

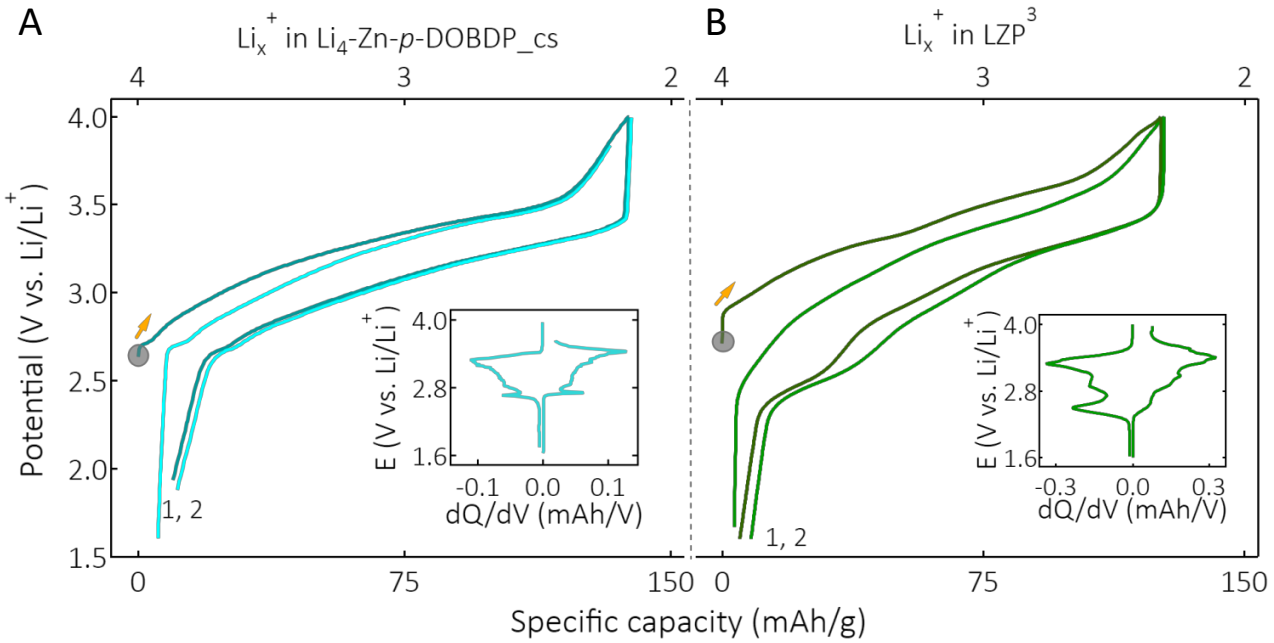


Figure 4. Electrochemical performance comparison of Li_4-Zn-*p*-DOBDP_cs and $L_{3.69}ZP^3$. Potential–composition profiles of reported Li_4-Zn-*p*-DOBDP_cs (A) and LZP^3 (B), measured in Li-metal half-cells, are shown along with their corresponding differential capacity (dQ/dV) plots as insets. For the $L_{3.69}ZP^3$ electrode, a galvanostatic rate corresponding to a one-electron exchange per formula unit over 20 hours (0.025 C) was applied. Electrodes were composed of 60 wt% active material, 30 wt% Super P carbon (C65), and 10 wt% PTFE. The electrolyte used was LP30, consisting of 1 M LiPF6 in a 1:1 (v/v) mixture of ethylene carbonate (EC) and dimethyl carbonate (DMC).

Rate and Cycling Capability of LZP^3

To assess potential kinetic limitations, C-rate tests were performed. Benefiting from its quasi-solid ionic conductivity, $L_{3.69}ZP^3$ demonstrated competitive rate performance, retaining 130 mAh/g at a low charge–discharge rate of 0.025C. Increasing the rate to 0.05C, 0.1C, 0.2C, 2C, and 4C resulted in specific capacities of 120 mAh/g, 109 mAh/g, 100 mAh/g, 80 mAh/g, and 70 mAh/g, respectively (**Figure 5A**). The gradual decrease in capacity at higher rates suggests that kinetic limitations, likely influenced by ion transport pathways, play a role in the material's rate-

dependent behavior. The $L_{3.69}ZP^3$ material exhibited good cycling stability, retaining over 99% of its initial capacity after 50 cycles at a rate of 0.2 C (**Figure 5B**). This stability is primarily attributed to the insoluble, polyanionic, and polymeric nature of the $L_{3.69}ZP^3$ framework, which helps prevent dissolution.

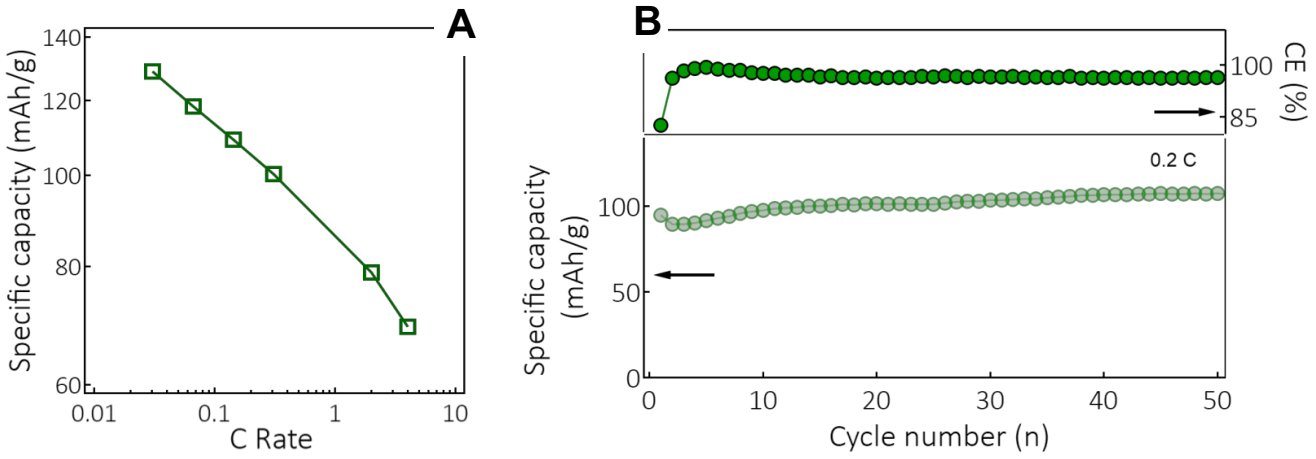


Figure 5. (A) Rate capability at C-rates ranging from 0.025 C to 4 C, and (B) cycling performance at 0.2 C of the $L_{3.69}ZP^3$ electrode in Li-metal half-cell configurations. Electrodes are composed of 60 wt% active material, 30 wt% Super P carbon, and 10 wt% PTFE, using LP30 electrolyte.

Conclusion

We have demonstrated a single-step, solvent-free solid-state approach for alkali-ion-containing metal-organic framework (MOF), addressing the challenges associated with multi-step processes that typically require solvents and precise optimization. Using a mechano-thermal method, we successfully synthesized the Li-ion MOF ($L_{3.69}ZP^3$), achieving direct lithiation during MOF formation. This approach enhances crystallinity of $L_{3.69}ZP^3$ while preserving its electrochemical performance (130 mAh/g at 3.2 V *vs.* Li^+/Li) and quasi-solid-state ionic conductivity (10^{-6} S/cm, at 303 K), comparable to conventionally synthesized multi-step methods. Beyond $L_{3.69}ZP^3$, this method may offer broader applicability to other transition-metal-based systems, making it a promising strategy for organic lithiation processes. These findings highlight the potential of solid-state synthesis in advancing alkali-ion-containing (metal-)organic cathode materials, offering a more sustainable and efficient route for next-generation energy storage applications.

Supporting Information

Supporting information is available along with this article ()

Acknowledgements

The major core of the work was funded through FWO and F.R.S.-FNRS under the Excellence of Science program (EOS 40007515). Partial support was received from the European Research Council under the European Union's Horizon 2020 research and innovation program (grant agreement No. 770870, MOOiRE – A.V.) as well as F.R.S.-

FNRS through F.4552.21-P grant. D.R., B.V.R, and X.L acknowledge F.R.S.-FNRS for Chargé de Recherché (CR) fellowship (grant agreement No. 40010410, 40023657 and 40010559). T.G., R.M., and G.C. acknowledges F.R.S.-FNRS for PhD fellowships.

Author Contributions

D.R., A.R., and A.V. conceived and designed the project. Solid-state mechano-thermal approach was initiated by D.R. and optimized by A.R. A.R. and D.R. have performed the major part of the experimental work, assisted by T.G., V.R.B., P.A., R.M., G.C., F.L. A.R., D.R., G.E, N.M. and Y.F., involved in the unit cell parameter determination. A.R., G.C. involved in SEM analysis. D.R. and A.R. performed conductivity measurements, assisted by T.G., V.R.B., P.A. R.M., F.L. involved in ICP analysis. All authors made iterative contributions and changes to the experiments during implementation and subsequent analysis, working collaboratively as a team. All authors contributed to the scientific discussion of the results as well as participated in the writing and approved the manuscript.

Keywords: *Li-ion cathode • Ionic conductivity • Metal-Organic Frameworks • one-pot solid state synthesis • mechano- thermal approach*

Conflict of Interest

The authors declare no conflict of interest.

References:

[1] D. Rambabu, A. E. Lakraychi, J. Wang, L. Sieuw, D. Gupta, P. Apostol, G. Chanteux, T. Goossens, K. Robeyns, A. Vlad, *J. Am. Chem. Soc.* **2021**, *143*, 11641–11650.

[2] M. Denis, H. Chevreau, P. Salcedo-Abraira, P. Moreau, N. Dupré, M. Paris, P. Poizot, T. Devic, *Mol. Syst. Des. Eng.* **2023**, *8*, 1030–1039.

[3] Z. Zhang, K. Awaga, *MRS Bull.* **2016**, *41*, 883–889.

[4] R. Zhao, Z. Liang, R. Zou, Q. Xu, *Joule* **2018**, *2*, 2235–2259.

[5] W. Wang, D. Chen, F. Li, X. Xiao, Q. Xu, *Chem* **2024**, *10*, 86–133.

[6] V. Shrivastav, S. Sundriyal, P. Goel, H. Kaur, S. K. Tuteja, K. Vikrant, K. H. Kim, U. K. Tiwari, A. Deep, *Coord. Chem. Rev.* **2019**, *393*, 48–78.

[7] Y. Zhang, J. Wang, P. Apostol, D. Rambabu, A. Eddine Lakraychi, X. Guo, X. Zhang, X. Lin, S. Pal, V. Rao Bakuru, X. Chen, A. Vlad, *Angew. Chemie - Int. Ed.* **2023**, *62*, DOI 10.1002/anie.202310033.

[8] Z. Zhang, H. Yoshikawa, K. Awaga, *J. Am. Chem. Soc.* **2014**, *136*, 16112–16115.

[9] M. E. Ziebel, C. A. Gaggioli, A. B. Turkiewicz, W. Ryu, L. Gagliardi, J. R. Long, *J. Am. Chem. Soc.* **2020**, *142*, 2653–2664.

[10] D. Sheberla, J. C. Bachman, J. S. Elias, C. J. Sun, Y. Shao-Horn, M. Dincă, *Nat. Mater.* **2017**, *16*, 220–224.

[11] D. M. D'Alessandro, *Chem. Commun.* **2016**, *52*, 8957–8971.

[12] Z. Wang, H. Tao, Y. Yue, *ChemElectroChem* **2019**, *6*, 5358–5374.

[13] D.-Y. Wang, R. Liu, W. Guo, G. Li, Y. Fu, *Coord. Chem. Rev.* **2020**, 213650.

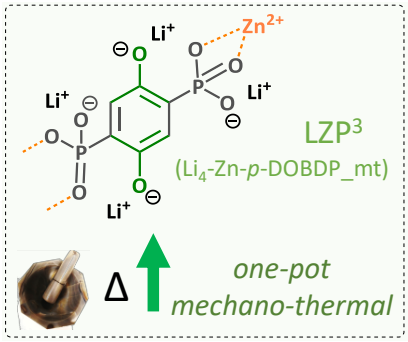
[14] A. Jouhara, N. Dupré, A. C. Gaillot, D. Guyomard, F. Dolhem, P. Poizot, *Nat. Commun.* **2018**, *9*, DOI 10.1038/s41467-018-06708-x.

[15] J. Wang, X. Guo, P. Apostol, X. Liu, K. Robeyns, L. Gence, C. Morari, J.-F. Gohy, A. Vlad, *Energy Environ. Sci.* **2022**, *15*, 3923–3932.

[16] V. R. Bakuru, P. Apostol, D. Rambabu, S. Pal, X. Lin, R. Markowski, T. Goossens, D. Tie, A. Kachmar, Y. Zhang, G. Chanteux, A. Vlad, *Energy Environ. Sci.* **2025**, DOI 10.1039/D4EE05701E.

[17] R. Russo, C. Davoisne, A. Urrutia, Y. Danten, C. Gatti, G. Toussaint, P. Stevens, C. Frayret, M. Becuwe, *ACS Appl. Polym. Mater.* **2023**, *5*, 9865–9875.

Entry for the Table of Contents



A solvent-free one-pot mechano-thermal route yields a Li-Zn(II) phosphono-phenolate MOF, with potential as a sustainable cathode material